BIOCELL
2023 47(7): 1611-1622

Tech Science Press

Exploring the attenuation mechanisms of *Dalbergia odorifera* leaves extract on cerebral ischemia-reperfusion based on weighted gene co-expression network analysis

Jinfang HU[1,#]; Jiangen AO[2,#]; Longsheng FU[1,#]; Yaoqi WU[1]; Feng SHAO[3]; Tiantian XU[1]; Mingjin JIANG[4]; Shaofeng XIONG[1]; Yanni LV[1,*]

[1] Department of Pharmacy, The First Affiliated Hospital of Nanchang University, Nanchang, 330006, China
[2] Department of Pharmacy, The Second Affiliated Hospital of Nanchang University, Nanchang, 330006, China
[3] Key Laboratory of Modern Preparation of TCM, Ministry of Education, Jiangxi University of Traditional Chinese Medicine, Nanchang, 330006, China
[4] Jiangxi Provincial Institute of Translational Medicine, The First Affiliated Hospital of Nanchang University, Nanchang, 330006, China

Key words: *Dalbergia odorifera* leaves, Serial affinity chromatography, WGCNA, Cerebral ischemia-reperfusion, TGF-β, SMADS

Abstract: Background: The attenuation function of *Dalbergia odorifera* leaves on cerebral ischemia-reperfusion (I/R) is little known. The candidate targets for the Chinese herb were extracted from brain tissues through the high-affinity chromatography. The molecular mechanism of *D. odorifera* leaves on cerebral I/R was investigated. **Methods:** Serial affinity chromatography based on *D. odorifera* leaves extract (DLE) affinity matrices were applied to find specific binding proteins in the brain tissues implemented on C57BL/6 mice by intraluminal middle cerebral artery occlusion for 1 h and reperfusion for 24 h. Specific binding proteins were subjected to mass-spectrometry to search for the differentially expressed proteins between control and DLE-affinity matrices. The hub genes were screened based on weighted gene co-expression network analysis (WGCNA). Then, predictive biology and potential experimental verification were performed for the candidate genes. The protective role of DLE in blood-brain barrier damage in cerebral I/R mice was evaluated by the leakage of Evans blue, western blotting, immunohistochemistry, and immunofluorescent staining. **Results:** 952 differentially expressed proteins were classified into seven modules based on WGCNA under soft threshold 6. Based on WGCNA, AKT1, PIK3CA, NOS3, SMAD3, SMAD1, IL6, MAPK1, TGFBR2, TGFBR1, MAPK3, IGF1R, LRG1, mTOR, ROCK1, TGFB1, IL1B, SMAD2, and SMAD5 18 candidate hub proteins were involved in turquoise module. TGF-β, MAPK, focal adhesion, and adherens junction signaling pathway were associated with candidate hub proteins. Gene ontology analysis demonstrated that candidate hub proteins were related to the TGF-β receptor signaling pathway, common-partner SMAD protein phosphorylation, etc. DLE could significantly reduce the leakage of Evans blue in mice with cerebral I/R, while attenuating the expression of occludin, claudin-5, and zonula occludens-1. Western blotting demonstrated that regulation of TGF-β/SMAD signaling pathway played an essential role in the protective effect of DLE. **Conclusion:** Thus, a number of candidate hub proteins were identified based on DLE affinity chromatography through WGCNA. DLE could attenuate the dysfunction of blood-brain barrier in the TGF-β/SMAD signaling pathway induced by cerebral I/R.

Introduction

Stroke is the first reason of death worldwide, with the increase in its incidence and the rate of mortality (Li *et al.*, 2019); it is also the first cause of death for Chinese people. Plants are naturally available source of food supplements or drugs for stroke therapy around the globe; for instance, leaves of *Ginkgo biloba* L. (Li *et al.*, 2021) or *Acanthopanax senticosus* (Wang *et al.*, 2020) are attractive materials for treating ischemic stroke. *Dalbergia odorifera* is mainly distributed in the Hainan and Guangdong provinces of China. *D. odorifera* is used for preparing drugs for treating cerebral infarction, thrombosis, and coronary heart diseases (Wang *et al.*, 2020). *D. odorifera* grows very slowly, for approximately 15 years until maturity; however, it has numerous fallen leaves. A large number of components have

*Address correspondence to: Yanni Lv, yannilv225@ncu.edu.cn
#Co-first authors: Jinfang Hu, Jiangen Ao, and Longsheng Fu contributed equally
Received: 01 January 2023; Accepted: 10 March 2023;
Published: 23 June 2023

Doi: 10.32604/biocell.2023.028684

been extracted from *D. odorifera* leaves (DO leaves) (Ma *et al.*, 2020), including a high content of flavone, isoflavone compounds, etc. One previous research group confirmed that 70% ethanol extract of *D. odorifera* leaves could exert a hypolipidemic effect on the hyperlipidemic rat model (Mei *et al.*, 2021). These studies were related to flavone compounds as the main component for treating cardiac and cerebral vascular diseases. However, little is known about the medicinal value, and the attenuation function of *D. odorifera* leaves on cerebral I/R.

Earlier, the high-affinity proteins were extracted through a method combined with serial affinity chromatography and shotgun proteomics analysis for traditional Chinese medicine (Lv and Fu, 2018). The integrated method was also applied to mine the target information for *D. odorifera* leaves. Weighted gene co-expression network analysis (WGCNA) is a method to describe correlation patterns between different genetic samples. WGCNA facilitates a complete investigation of the relationship between genes and their phenotypes (Sonoda *et al.*, 2019) and aids in screening for key genes for the identification of candidate biomarkers or therapeutic targets (Shuai *et al.*, 2021). Here, a number of differentially expressed proteins were obtained from the affinity resin of *D. odorifera* leaves extract (DLE) for cerebral I/R. The WGCNA-based approach was used to identify candidate protein modules associated with differentially expressed proteins to study the role and mechanisms of DLE on cerebral I/R.

Materials and Methods

Materials and chemicals

DO leaves were collected from the Jianfengling area, Sanya City, Hainan Province, China. A voucher specimen (No. 20200123) was stored in the Key Laboratory of Modern Preparation of Traditional Chinese Medicine, Ministry of Education, Jiangxi University of Traditional Chinese Medicine, China.

Preparation of 70% ethanol extract of Dalbergia odorifera leaves

The *D. odorifera* (500 g) extract (DLE) was prepared using air-dried leaves and 70% ethanol under a refluxing extraction (2 h, 5 L × twice) and filtered. The combined extracts were then rotary evaporated at 45°C and lyophilized (Shao *et al.*, 2016). The ethanol extract was dissolved with 30% methanol and stored at 4°C until use. Rutin was accurately weighed to 5.41 mg and dissolved with 30% methanol to obtain the reference solution (0.541 mg/mL). The general flavonoid content of DLE was determined using the colorimetric method. Rutin was used as the standard. The absorbance of samples was measured at 500 nm.

HPLC analysis for general flavones of 70% ethanol extract of Dalbergia odorifera leaves

The air-dried leaves of *D. odorifera* (100 g) were used to prepare 70% ethanol under refluxing extraction (2 h, 1 L × twice) and filtered. The combined extracts were then rotary evaporated at 45°C and lyophilized. The extract ethanol was dissolved with methanol and stored at 4°C until use. Separation was performed on a 250 × 4.6 mm Phenomenex C18 (5 μm, California, USA) at 30°C, and the UV absorbance was monitored at 260 nm on Agilent 1100. The flow rate was 1.0 mL/min. The solvent system used the improved method published earlier (Li *et al.*, 2016): composed of acetonitrile (A) and 0.1% phosphoric acid (B) using an optimized gradient program: 0–10 min 35% A; 10–15 min 35%–48% A; 15–30 min 48%–49% A. The injection volume was 10 μL. The DLE in 70% ethanol was accurately weighed and dissolved in a 2 mL volumetric flask with methanol. The final solution was filtered through a 0.22 μm microfilter to obtain a reference solution.

Animals and ischemia-reperfusion

C57BL/6J male mice (8~10 weeks old; weighing 18~22 g) were purchased from the College of Veterinary Medicine YanZhou University of Comparative Medicine (certificate No. SCXK (SU) 2022-0009) and placed in the laboratory of the First Affiliated Hospital of Nanchang University. All efforts were made to minimize animal suffering and the number of animals used. C57BL/6 mice were anesthetized with 1.2% isoflurane during the ischemia period. The environment temperature was maintained at 37°C during the ischemia and recovery period. A blunt tip 6–0 nylon monofilament was inserted into the neck vessel and advanced 8–10 mm forwards. After 1 h of occlusion, the monofilament was withdrawn, then 24 h reperfusion was immediately followed. Mice in the sham-operated group underwent the same surgical incision, but the nylon monofilament was not advanced into the internal carotid artery. Animals whose blood flow dropped below 30% of pre-ischemia levels were used for further study.

Animal groups

The administration dose was determined according to earlier studies (Mei *et al.*, 2021), while the dose given to rats was converted corresponding to that of mice. The DLE treatment group was administered intragastrically with 0.6, 1.2, or 2.4 g/kg 1 h of the onset of cerebral ischemia and every 24 h during the experimental period, whereas the sham-operated group was administered intragastrically with a solution of equivalent volume NaCl. Mice were randomly categorized into six groups (8 mice for each group): (1) sham-operated mice (sham); (2) mice exposed to 1 h of ischemia and 24 h of reperfusion stroke (I/R); (3) mice exposed to 1 h of ischemia and 24 h of reperfusion stroke and treatment with a low dose of DLE (0.6 g/kg) (I/R+0.6 g/kg DLE); (4) mice exposed to 1 h of ischemia 24 h of reperfusion stroke, and treated with a middle dose of DLE (1.2 g/kg) (I/R+1.2 g/kg DLE); (5) mice exposed to 1 h of ischemia and 24 h of reperfusion stroke and treatment with a high dose of DLE (2.4 g/kg) (I/R+2.4 g/kgDLE); (6) 1 h of ischemia stroke, 24 h of reperfusion stroke and treatment with 10 mg/kg nimodipine (I/R+10 mg/kg NM) (Lv and Fu, 2018). At the end of the cerebral I/R period, the mice were examined for leakage of Evans blue, immunostaining, immunohistochemistry, and western blot analysis.

Preparation of mice brain lysate and Dalbergia odorifera leaves extract affinity resin

The epoxy-activated sepharose^{TM}6B (EAS-6B) was from GE Healthcare, Delaware, USA. The affinity resin was prepared using the earlier published formula (Lv and Fu, 2018). The leaf extract was dissolved in DMSO, then added into EAS-6B, which was fully expanded before 300 mmoL, soaked at 25°C for 24 h, lightly filtered with double distilled water for 15 min, drained, and preserved at 4°C under dry conditions. Brain tissue homogenates were centrifuged at 9,500 rpm for 10 min and 50,000 rpm for 30 min and diluted in lysate buffer to a total protein concentration of about 7 mg/mL. The homogenate was shaken gently at 4°C for 4 h with an affinity medium of 60 mL. This step was repeated five times. Sodium dodecyl sulfate-polyacrylamide gel electrophoresis (SDS-PAGE; Bio-Rad, California, USA) was performed with the supernatant solution, and silver staining was performed using Quantity One software 4.6.2. The proteins were identified in the mass spectrometry database from the SEQUEST output file.

Screened out differential expressed proteins

Limma and Impute package in R software (4.0.4) were installed, and each group of data in section '*Materials and chemicals*' to matrix were processed, and the missing matrix filled. The $\log_2$ value of the data set was taken and corrected to the same level. The up-regulated and down-regulated proteins compared between control-affinity proteins or DLE-affinity proteins were screened out, and with differentially expressed proteins, the truncated values were set to $\log_2 F \geq 1$ and p-value < 0.05. The volcano map and heat map were used to display the differential expressed proteins. In R software, define $\log_2 FC$ as the x-axis and the p-value as the y-axis to draw the volcano map.

Construction of weighted gene co-expression network

The screened differential expressed proteins were processed in R Studio 4.0.4 software using the WGCNA package to construct co-expression networks. First, the scale-free topology model Fitsigned R^2 and mean connectivity were calculated to determine the soft threshold (power) for the protein co-expression network. According to the compatible soft threshold, the degree of fitting was considered between the chosen genes and putative proteins. Then, the protein expression similarity matrix was converted into an adjacency matrix; then, the adjacency matrix was converted into a topological overlap matrix (TOM). The TOM assay was applied to convert the protein expression similarity matrix to the adjacency matrix. Hierarchical clustering based on TOM was constructed using a dynamic tree-cutting algorithm, Connectivity Cut was set as 1,000, and the preset number of modules was set as height 0.8 and minsize 3. After determining the protein modules, the eigenvector values of each module were calculated for clustering analysis, and the modules that were closer were merged into new modules. Genes with similar expression patterns were considered specific branch modules marked with a unique color.

Gene ontology (GO) enrichment and Kyoto Encyclopedia of Genes and Genomes (KEGG) singling pathway analysis

GO enrichment and KEGG signaling pathway analysis were performed on gene modules using the annotation and database DAVID (https://david.ncifcrf.gov/). Cut-off criteria were set as count ≥10, and $p < 0.05$ was chosen as the critical value, while false discovery rate (FDR) correction was applied for multiple test corrections. The significance level was set to 0.05, and classification information was set to functional classification and human annotation. The biological processes (BP), cellular components (CC), and molecular functions (MF) module were applied to analyze the biological function of proteins, and $-\text{Log}_2\text{FC}$ was defined to make the biological function map for the y-axis. The protein function was enriched by Fisher's rectified p-value ≤ 0.01, and the signaling pathways with similar functions were classified according to the enrichment score.

Evaluation of blood-brain barrier permeability

0.1 mL/10 g of 2% Evans blue (Sigma Aldrich Co., Saint Louis, USA) was administered through a caudal vein 2 h before euthanasia. To quantitatively measure the leakage of Evans blue, the ipsilateral hemisphere was homogenized and centrifuged at 12,000 rpm for 20 min. The absorbance of the supernatant was measured by spectrophotometer at 620 nm, and the concentration of Evans blue was determined.

Histological assessment of tight junction proteins

The I/R brain tissue was soaked with 4% paraformaldehyde for 24 h and then embedded with paraffin after dehydration. Anti-occludin, claudin-5, and zonula occludens-1 (ZO-1; rabbit polyclonal IgG, 1:50, Zyemd, Wuhan, China) antibodies were incubated with brain tissues. The occludin, claudin-5, and ZO-1 positive boundaries were quantitatively measured in a 20 μm enlarged view. The data were expressed as a percentage of the number of positive boundaries in cerebral I/R mice.

Immunofluorescent staining of tight junction proteins

Brain tissues in each group were cut into 5 mm pieces, washed with phosphate-buffered saline, immobilized with cold ethanol at 4°C for 10 min, and fixed with 10% normal goat serum, 3% bovine serum albumin, and 0.1% Triton X-100 in phosphate-buffered saline for 1 h. Then, the tissue pieces were incubated with the occludin (ab216327, Abcam, Cambridge, UK), claudin-5 (ab131259, Abcam, Cambridge, UK), and ZO-1 (ab96587, Abcam, Cambridge, UK) primary antibodies (IF for 1:100) for 48 h at 4°C. Brain tissues were incubated overnight with Alexa Fluor® 488 conjugated donkey anti-goat IgG (H+L) antibody (ab150129, Abcam, Cambridge, UK; 1:2000) at 4°C, while the nuclei of all cells were washed and incubated with 4′6-diamidino-2-phenylindole (DAPI, ab104139, Abcam, Cambridge, UK; 1:1000). Briefly, confocal images were used to observe the fluorescence images of each group (ChemiScope 6100BZ, Shanghai, China).

Western blot analysis

The protein concentration was determined by the BCA method. The membranes separated by SDS-PAGE

electrophoresis were transferred onto polyvinylidene difluoride membranes. The membranes were incubated for blocking with 5% nonfat dry milk at room temperature for 2 h, then incubated with anti-leucine-rich α-2 glycoprotein 1 (LRG1; ab178698, Abcam, Cambridge, UK), anti-transforming growth factor beta 1 (TGF-β1; ab235578, Abcam, Cambridge, UK), rho-associated protein kinase1 (ROCK1; ab134181, Abcam, Cambridge, UK), phosphorylated-mechanistic target of rapamycin (p-mTOR; ab109268, Abcam, Cambridge, UK), mTOR (ab13490, Abcam, Cambridge, UK), anti-phosphorylated-SMAD2 (p-SMAD2; ab280888, Abcam, Cambridge, UK), anti-SMAD2 (ab40855, Abcam, Cambridge, UK), anti-p-SMAD3 (ab52903, Abcam, Cambridge, UK), anti-SMAD3 (ab40854, Abcam, Cambridge, UK), anti-occludin (ab216327, Abcam, Cambridge, UK), anti-claudin-5 (ab131259, Abcam, Cambridge, UK), anti-ZO-1 (ab276131, Abcam, Cambridge, UK), and β-actin (ab8226, Abcam, Cambridge, UK) primary antibodies (1:1000), and then incubated with secondary antibody (HRP-conjugated secondary antibody, 1:2000, ab6728; Abcam, Cambridge, UK) for 50 min. Enhanced chemiluminescence was used for image capture through a bioimage analysis system (Bio-Rad, California, USA).

Statistical analysis

All values are expressed as mean ± SD. The data were analyzed based on a two-tailed student's *t*-test (two groups) or a two-way ANOVA followed by Bonferroni's test (three or more groups) through Graph Prism 5.2. The significance level was set at $p < 0.05$ and $p < 0.01$.

Results

High-performance liquid chromatography (HPLC) detection of general flavones from Dalbergia odorifera leaves

HPLC method was used for the detection of general flavones from *D. odorifera* leaves. At wavelengths of 211, 254, 270, and 360 nm, the absorption peak of fingerprint of general flavonoids of 70% ethanol extract of *D. odorifera* leaves was detected (Fig. 1). The mass proportion of general flavonoids was 140.74 ± 2.16 mg/g (Fig. 1).

Identification of differential expressed proteins

Eight decreased expression protein bands were singled out from cerebral I/R mice treated with control-affinity resin or DLE (70% ethanol extract of *D. odorifera* leaves)-affinity resin via series affinity chromatography (Figs. 2A and 2B). The identified proteins from the control affinity resin were compared with those protein bands from DLE-affinity resin. In total, 2,190 proteins were identified (Suppl. Tables S1 and S2). For subsequent analysis, 952 differential expression proteins were screened (log_2Fold Change > 0.5, adj.*p*.Val < 0.05) (Suppl. Table S3 and Suppl. Fig. S1). The comparison revealed 644 up-regulated and 308 down-regulated differentially expressed proteins on proteins identified from the control affinity resin.

Co-expression protein modules extraction based on weighted gene co-expression network analysis

A total of 952 differential expressed proteins were screened by WGCNA. The parameter β was screened between 1 and 20, and the optimal soft threshold value was determined as 6. When the soft threshold power was set as 6, the degree of fitting was scale-free R^2 = 0.95 and trunc.R^2 = 0.95 (Figs. 3A and 3B). According to the soft threshold value, the network approximated the real biological network, and it amounted to the power law distribution. The relationship matrix was translated into an adjacency matrix, and finally, seven expression modules were constructed (Figs. 3D and 3E). Co-expression modules were constructed based on the TOM. The resulting protein tree and corresponding module colors are shown in Fig. 3B, of which the turquoise module had the strongest internal interaction (Fig. 3F).

Prediction through gene ontology biological function and kyoto encyclopedia of genes and genomes signaling pathway analyses

Hub proteins identified via WGCNA were (protein name symbols name represented for protein name) AKT1, PIK3CA, NOS3, SMAD3, SMAD1, ATK1, MAPK1, TGFBR2, TGFBR1, MAPK3, IGF1R, LRG1, mTOR, ROCK1, TGFB1, TGF1, SMAD2, SMAD5 (Fig. 4A). Candidate proteins obtained from hub protein module via WGCNA were subjected to BP, CC, and MF analyses, and $-Log_{10}$FDR was defined to make the biological function map for the y-axis. BP was related to TGF-β receptor signaling pathway, common-partner SMAD protein phosphorylation, pathway-restricted SMAD protein phosphorylation, etc. CC was associated with positive regulation of pathway-restricted SMAD protein phosphorylation, SMAD protein complex, SMAD2-SMAD3 protein complex, etc. MF was related to the transcription factor complex, inhibitory-SMAD (I-SMAD) binding, SMAD binding, etc. (Fig. 4B). The hub proteins were associated with KEGG signaling pathways as TGF-β signaling pathway, mitogen-activated protein kinases (MAPK) signaling pathway, focal adhesion, adherens junction, etc. (Fig. 4C).

Dalbergia odorifera leaves extract attenuated blood-brain barrier dysfunction

The content of the Evans blue inside cerebral I/R brain tissue was examined to assess the effect of DLE on the blood-brain barrier permeability quantitatively. Quantitative content revealed DLE treatment significantly reduced Evans blue leakage (low, middle, high dose: 2.21 ± 0.24 mg/g, $p < 0.01$, 1.94 ± 0.21 mg/g, $p < 0.01$, 1.52 ± 0.24 mg/g, $p < 0.01$) compared with the cerebral I/R group (2.89 ± 0.26 mg/g, $p < 0.01$, sham: 0.25 ± 0.29), and 10 mg/kg nimodipine (1.54 ± 0.27 mg/g, $p < 0.01$) had the same effect (Fig. 5).

This linear shape along the tight junction proteins of blood vessels reduced with lower expression in response to I/R (Fig. 6A), with a weaker signal strength of occludin, claudin-5, and ZO-1 (occludin: 10.49 ± 8.77, $p < 0.01$; claudin-5: 7.49 ± 5.21, $p < 0.01$; ZO-1: 7.78 ± 10.15, $p < 0.01$; sham: occludin: 51.49 ± 9.47; claudin-5: 47.59 ± 6.42; ZO-1: 56.88 ± 8.49). The DLE dose-dependent improved the pathological injury of brain tissues in cerebral I/R mice by strengthening immunohistochemical expression intensity of tight junctions (low, middle, high dose DLE: occludin: 14.59 ± 7.44, $p < 0.01$, 18.48 ± 8.45, $p < 0.01$, 28.47 ± 5.49, $p < 0.01$; claudin-5: 14.59 ± 6.34, $p < 0.01$, 26.47 ± 4.17,

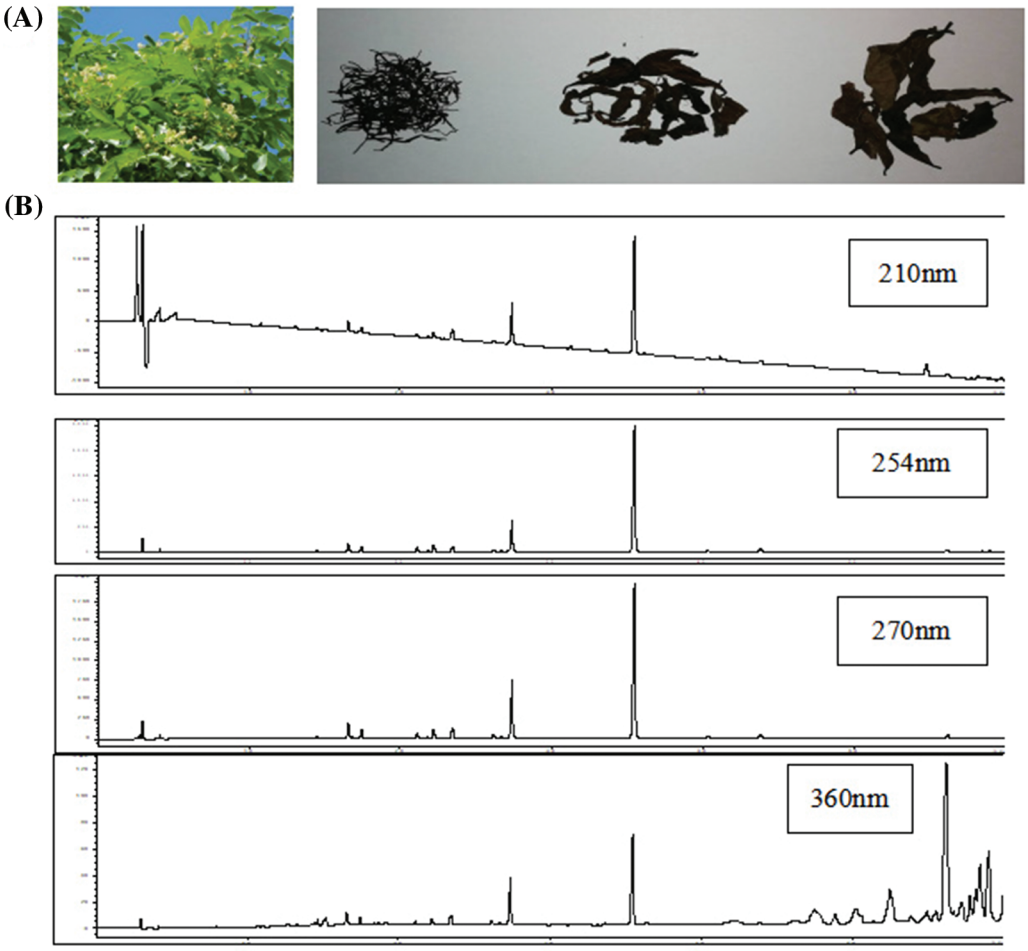

(C)

Medicinal parts	Extract solution	Extract yield %	General flavonoids mg/g
leaves	70% ethanol	22.12	140.74±2.16

FIGURE 1. High-performance liquid chromatography (HPLC) for the determination of general flavones of *Dalbergia odorifera* leaves. (A) The shape of fresh and air-dried *D. odorifera* leaves; (B) HPLC fingerprint of general flavonoids of 70% ethanol extracted from *D. odorifera* leaves; (C) The mass proportion of general flavonoids in *D. odorifera* leaves.

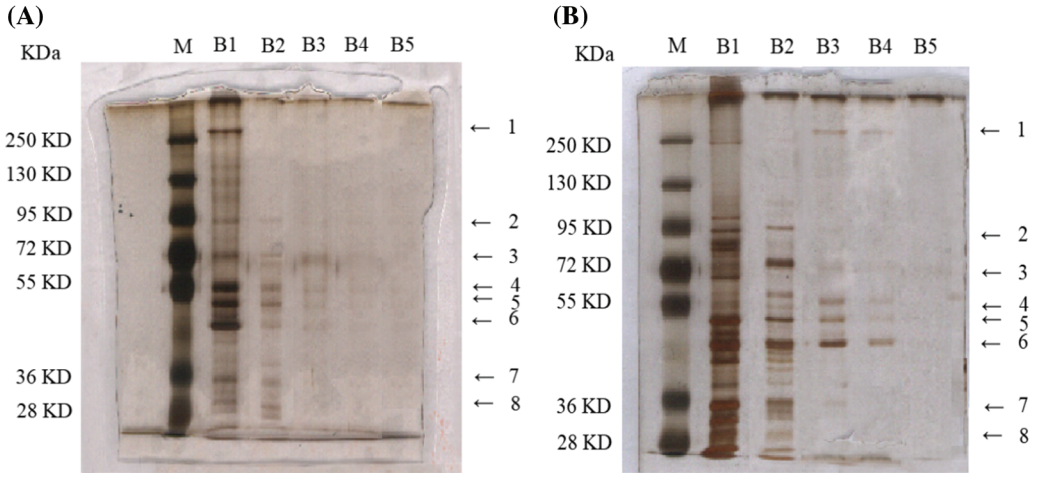

FIGURE 2. Differential concentration expressed protein bands from mice after 1 h of ischemia and 24 h of reperfusion, based on serial affinity chromatography. (A) Silver staining bands from control-affinity resin via serial affinity chromatography. (B) Silver staining bands from DLE-affinity resin via serial affinity chromatography. The protocol was analyzed with five repeats. Lane M: Marker; Lane B1–B5: After the synthesis of DLE affinity resin, the resin was subjected to incubation with brain tissue homogenates, repeated five times. Lane B numbered 1–5, represents the protein samples from each incubation via silver staining.

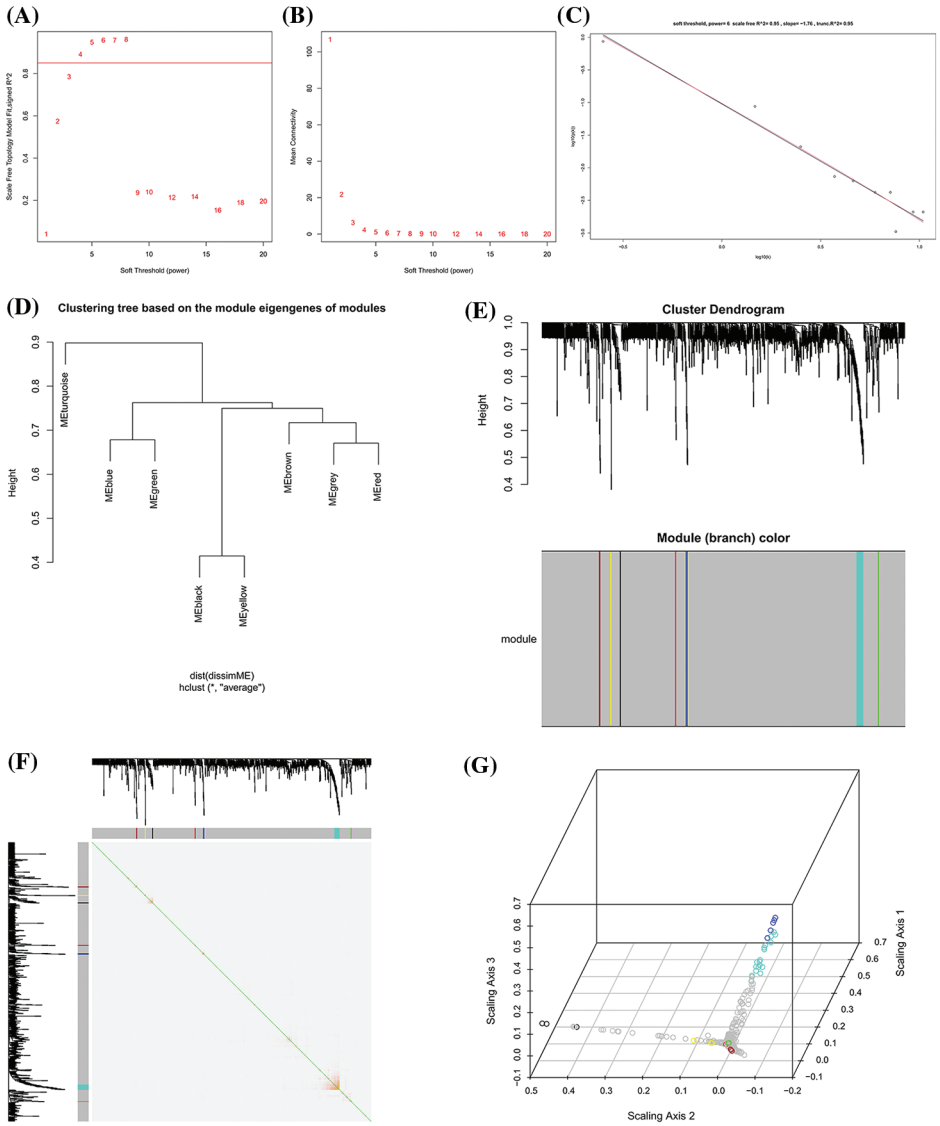

FIGURE 3. Co-expression protein modules extraction based on weighted gene co-expression network analysis (WGCNA). (A) Soft threshold determination of the WGCNA. (B) Soft threshold power based on the average connectivity. (C) Under the Soft threshold 6, the scale-free network fitted with the ideal curve. (D) Hierarchical clustering dendrograms of identified protein modules with co-expressed proteins. (E) Cluster genes via hierarchical clustering. Different color represents a different module but a similar set of proteins. (F) Correlation matrix between protein modules of adjacency differences adjacency. Each row corresponds to a module feature protein, and each column corresponds to a particular feature. The left and top bars correspond to each row or column. (G) 3D represented each row or column of protein modules.

$p < 0.01$, 37.09 ± 3.84, $p < 0.01$; ZO-1: 12.47 ± 8.55, $p < 0.01$, 19.09 ± 8.49, $p < 0.01$, 42.35 ± 9.78, $p < 0.01$, Figs. 6A and 6B), the integrity of vascular vessel expression was restored to some extent.

Tight junctions were continuous and well organized in the sham-operated blood vessel edge through immunofluorescent staining (Figs. 6C–6F). After stimulation with I/R, occludin, claudin-5, and ZO-1 revealed structural disturbance with reduced fluorescence compared with the sham-operated group. Moreover, immunocytochemical staining of tight junction proteins along the blood vessel edge was restored to a higher fluorescence expression intensity in response to the treatment of DLE. After treatment with DLE, the protein expression of LRG1, TGF-β1, p-SMAD2/SMAD2, p-SMAD3/SMAD3 were downregulated, while the expressions of ROCK1, p-mTOR/mTOR, occludin, claudin-5, ZO-1 were up-regulated (I/R+2.4 g/kg DLE: LRG1: 1.24 ± 0.02, $p < 0.01$; TGF-β1: 1.17 ± 0.05, $p < 0.01$; p-SMAD2/SMAD2: 1.24 ± 0.04, $p < 0.01$; p-SMAD3/SMAD3: 1.21 ± 0.03, $p < 0.01$, ROCK1: 1.44 ± 0.04, $p < 0.01$, p-mTOR/mTOR: 1.46 ± 0.07, $p < 0.01$, occludin: 1.45 ± 0.09, $p < 0.01$, claudin-5: 1.47 ± 0.04, $p < 0.01$, ZO-1: 1.45 ± 0.04, $p < 0.01$, Fig. 7) compared with those of the I/R group (LRG1: 1.72 ± 0.03, $p < 0.01$; TGF-β1: 1.66 ± 0.04, $p < 0.01$; p-SMAD2/SMAD2: 1.79 ± 0.07, $p < 0.01$; p-SMAD3/SMAD3: 1.74 ± 0.05, $p < 0.01$, ROCK1: 1.00 ± 0.05, $p < 0.01$, p-mTOR/mTOR: 1.00 ± 0.05, $p < 0.01$, occludin: 1.00 ± 0.03, $p < 0.01$, claudin-5: 1.02 ± 0.04, $p < 0.01$, ZO-1: 1.02 ± 0.07, $p < 0.01$, Fig. 7).

(A)

Gene symbol	Protein name	Gi no. (Uniprot)	No. of unique peptides	MW	pI	GEO Profile	LogFC
AKT1	thymoma viral proto-oncogene 1	P31749_human	15	55686 Da	4.21	1425711_a_at	5.482
PIK3CA	phosphatidylinositol-4,5-bisphosphate 3-kinase catalytic subunit alpha	P42336_human	15	124284 Da	4.58	1429434_at	7.489
NOS3	nitric oxide synthase 3	P29474_human	14	133275 Da	5.03	205581_s_at	-2.485
SMAD3	SMAD family member 3	P84022_human	17	48081 Da	7.74	218284_at	-5.264
SMAD1	SMAD family member 1	Q15797_human	20	52260 Da	6.34	210993_s_at	-3.401
IL6	interleukin 6	P05231_human	12	23718 Da	6.89	205207_at	-2.154
MAPK1	mitogen-activated protein kinase 1	P28482_human	15	41390 Da	10.58	224621_at	-2.014
TGFBR2	transforming growth factor beta receptor 2	P37173_human	18	64568 Da	7.12	208944_at	-6.587
TGFBR1	transforming growth factor, beta receptor I	P36897_human	21	55960 Da	5.84	1420893_a_at	-4.698
MAPK3	mitogen-activated protein kinase 3	Q16644_human	22	43136 Da	2.59	101834_at	-4.158
IGF1R	insulin-like growth factor I receptor	P08069_human	19	154793 Da	4.35	102224_at	-2.584
LRG1	leucine-rich alpha-2-glycoprotein 1	P02750_human	16	38178 Da	3.58	1417290_at	-7.695
MTOR	mechanistic target of rapamycin	P42345_human	37	288892 Da	3.49	202288_at	-2.489
ROCK1	Rho associated coiled-coil containing protein kinase 1	Q13464_human	26	158175 Da	3.25	1450994_at	-8.457
TGFB1	transforming growth factor beta 1	P01137_human	28	44341 Da	4.38	203085_s_at	-5.848
IL1B	interleukin 1 beta	P01584_human	59	30748 Da	4.19	39402_at	-5.994
SMAD2	SMAD family member 2	Q15796_human	42	52306 Da	6.89	203076_s_at	-5.487
SMAD5	SMAD family member 5	Q99717_human	44	52258 Da	7.64	235451_at	-4.596

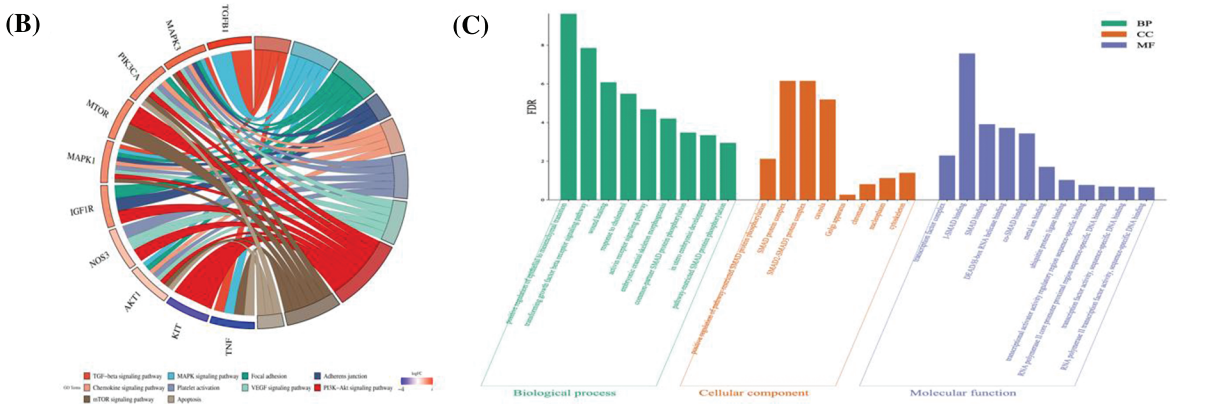

FIGURE 4. Prediction of hub proteins screened via weighted gene co-expression network analysis (WGCNA) for Gene Ontology (GO) biological function and kyoto encyclopedia of genes and genomes (KEGG) signaling pathway. (A) Hub proteins screened via WGCNA. (B) GO annotation analysis. The top 10 most enriched GO terms respectively represented biological processes (BP), cellular components (CC), and molecular functions (MF). The x-axis represents the enrichment annotation, and the y-axis represents $-\text{Log}_{10}$FDR. (C) The chord figure represents the top 10 enriched KEGG signaling pathways and 10 included proteins. The weight in the chord figure is associated with the $-\text{Log}_{10}$FC relevance protein with signaling pathway enriched through KEGG.

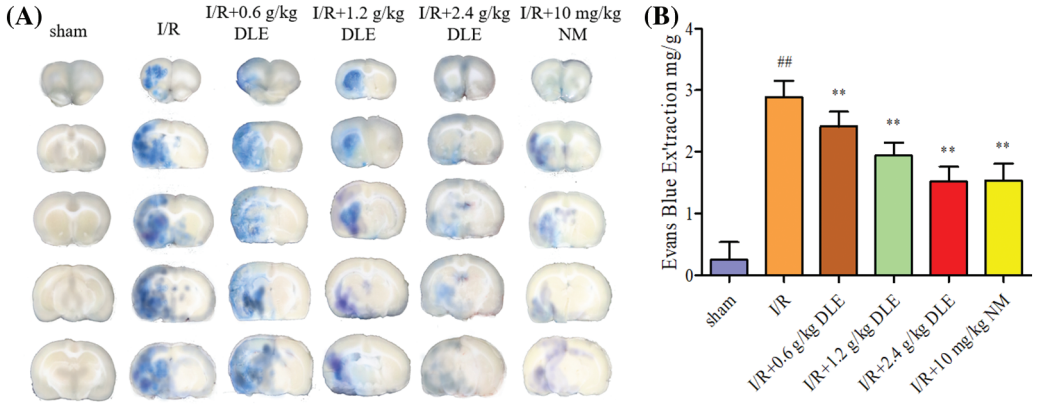

FIGURE 5. Attenuation mechanism of *D. odorifera* leaves extract (DLE) on blood-brain barrier permeability in cerebral ischemia-reperfusion (I/R) mice. (A) Representative appearance brain of Evans blue in 1 h of ischemia, 24 h of reperfusion mice. Mice were randomly categorized into six groups: (1) sham-operated mice (sham); (2) mice exposed to 1 h of ischemia, 24 h of reperfusion stroke (I/R); (3) mice exposed to I/R and treatment with 0.6 g/kg DLE (I/R+0.6 g/kg DLE); (4) mice exposed to I/R and treatment with 1.2 g/kg of DLE (I/R+1.2 g/kg DLE); (5) mice exposed to I/R and treatment with 2.4 g/kg of DLE (I/R+2.4 g/kg DLE); (6) mice exposed to I/R and treatment with 10 mg/kg nimodipine (I/R +10 mg/kg NM). (B) Analysis of Evans blue content by quantitative spectrophotometry. The results were presented as eight independent experiments. The data were averages with S.D., n = 8. $^{\#}p < 0.05$, $^{\#\#}p < 0.01$ *vs.* sham-operated mice, $^{*}p < 0.05$, $^{**}p < 0.01$ *vs.* 1 h of ischemia, 24 h of reperfusion stroke.

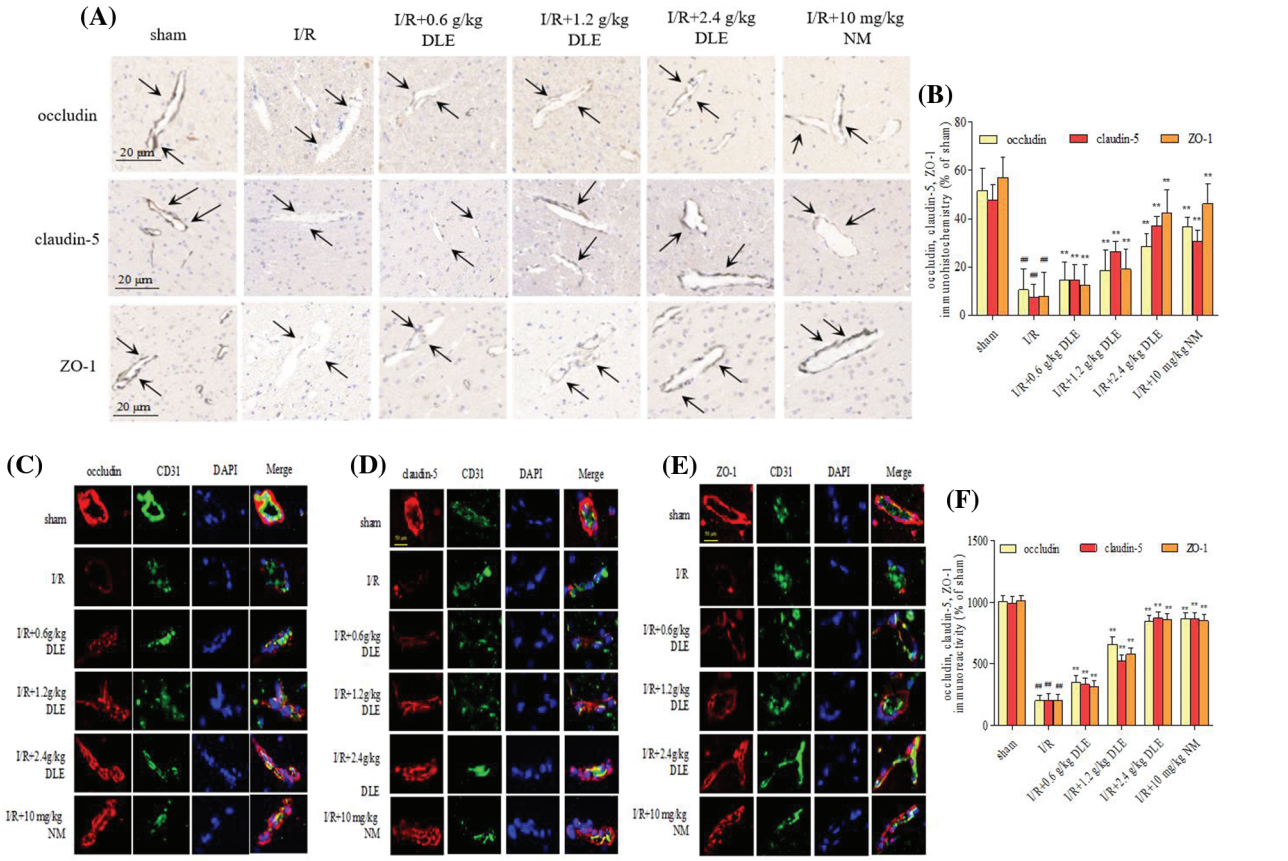

FIGURE 6. Effect of *D. odorifera* leaves extract (DLE) on immunohistochemistry staining changes in tight junctions in brain tissues exposed to 1 h of ischemia, 24 h of reperfusion stroke mice. (A) The ischemia-reperfusion (I/R) fields were observed under ChemiScope 6100BZ, bar = 20 μm. Mice were randomly categorized into six groups: (1) sham-operated mice (sham); (2) mice exposed to 1 h of ischemia, 24 h of reperfusion stroke (I/R); (3) mice exposed to I/R and treatment with 0.6 g/kg DLE (I/R+0.6 g/kg DLE); (4) mice exposed to I/R and treatment with 1.2 g/kg of DLE (I/R+1.2 g/kg DLE); (5) mice exposed to I/R and treatment with 2.4 g/kg of DLE (I/R+2.4 g/kg DLE); (6) mice exposed to I/R and treatment with 10 mg/kg nimodipine (I/R+10 mg/kg NM). (B) The tight junction positive boundaries were measured. The data are presented as the percentage of positive boundaries in the cerebral I/R mice. The data were the mean value with SD, n = 8. $^{\#}p < 0.05$, $^{\#\#}p < 0.01$ *vs.* sham-operated mice, $^{*}p < 0.05$, $^{**}p < 0.05$ *vs.* 1 h of ischemia, 24 h of I/R. (C–E) Representative immunofluorescence staining of occludin (red), claudin-5 (red), and ZO-1 (red) in I/R mice. The nucleus was stained with DAPI (blue), and the vascular endothelial cells with CD31 (green). Confocal microscopy images were acquired, bar = 50 μm. The images represent nine individual views from each group. (F) The expression of TGF-β, p-SMAD2, SMAD2, p-SMAD3, and SMAD3, and β-actin in I/R-treated mice were detected via western blotting. The data were the mean value with S.D., n = 8, $^{\#}p < 0.05$, $^{\#\#}p < 0.01$ *vs.* the sham-operated mice, $^{*}p < 0.05$, $^{**}p < 0.01$ *vs.* 1 h of ischemia, 24 h of I/R.

Discussion

Plant parts like rhizome and pith are medicinal plants, whereas leaves, seeds, flowers, and fruits from these plants are all resources that could be developed into food or medicine. Many kinds of leaves from traditional Chinese plants can be used as commercial food or medicine. Previous studies have isolated ~150 components from *D. odorifera* leaves, containing general flavonoids, exhibiting the highest antioxidant activity in scavenging DPPH·, O^{2-}, ·OH, H_2O_2, and NO^{2-} (Li and Chen, 2013). General flavonoid components, such as biochanin A and genistein are in abundance and are the main active components in *D. odorifera* leaves (Li *et al.*, 2016). Biochanin A mitigated dyslipidemia in hyperlipidemic, atherosclerosis, and diabetes in rats (Sarfraz *et al.*, 2020), whereas genistein exerted good hypolipidemic effects on clinical patients and mice (Yang *et al.*, 2021a). Other ingredients, such as tectorigenin and prunetin, were also reported for their pharmaceutical value. Given the amounts of active ingredients contained in *D. odorifera* leaves and the potential rapid economic benefits, we had good reason to examine the medicinal value of *D. odorifera* leaves.

The alcohol extraction method yielded a relatively high content of general flavonoids from *D. odorifera*. leaves. Previously, an integrated approach was successfully used for extracting special binding proteins from Chinese herbal compounds. The integrated method could reveal a more complex protein map for *D. odorifera* leaves. The identified proteins from the control affinity resin and DLE-affinity resin were compared. The identified differentially expressed proteins were involved in a large network, and a large amount of information was contrary to the accurate experimental verification. WGCNA is suitable for complex transcriptome data, also mapping regulatory networks among gene sets, and identifying key regulatory genes.

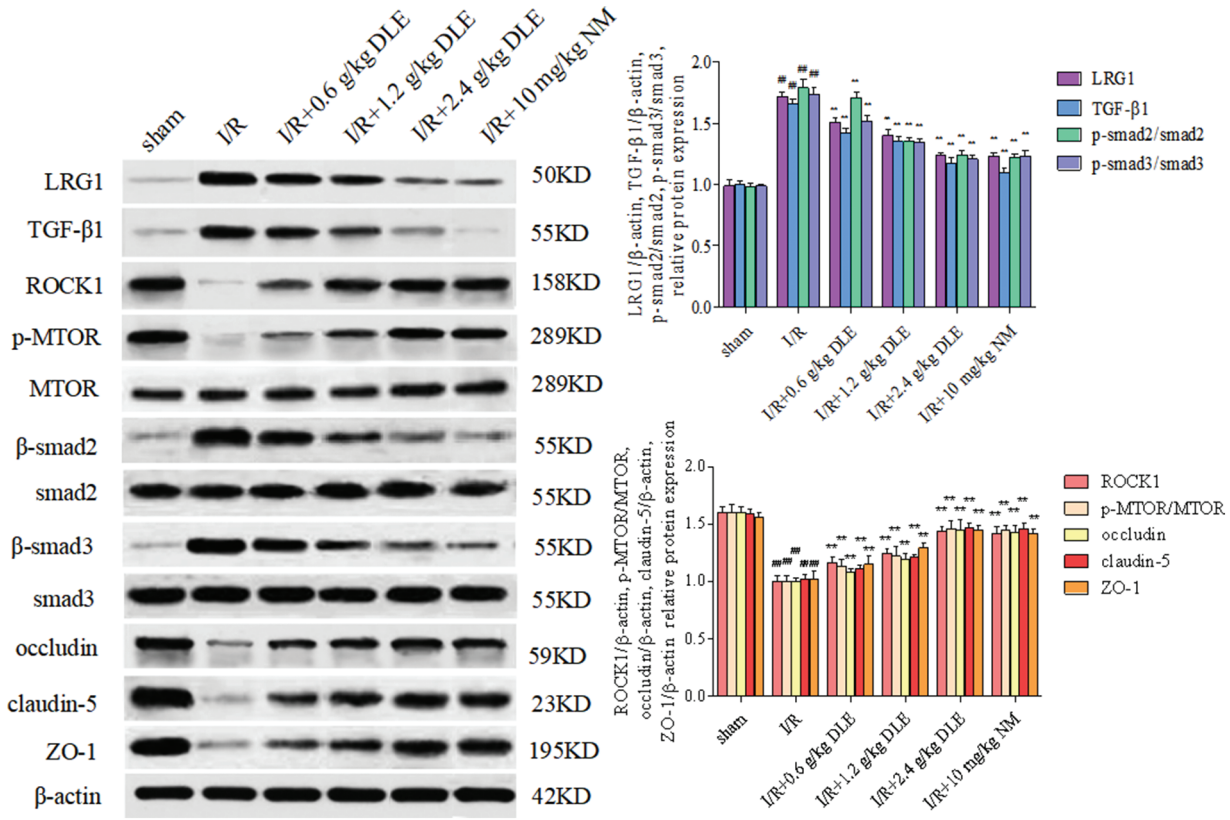

FIGURE 7. Western blot expression of the treatment of *D. odorifera* leaves extract (DLE) on tight junctions in brain tissues exposed to 1 h of ischemia, 24 h of reperfusion stroke mice. Mice were randomly categorized into six groups: (1) sham operated mice (sham); (2) mice exposed to 1 h of ischemia, 24 h of reperfusion stroke (I/R); (3) mice exposed to I/R and treatment with 0.6 g/kg DLE (I/R+0.6 g/kg DLE); (4) mice exposed to I/R and treatment with 1.2 g/kg of DLE (I/R+1.2 g/kg DLE); (5) mice exposed to I/R and treatment with 2.4 g/kg of DLE (I/R+2.4 g/kg DLE); (6) mice exposed to I/R and treatment with 10 mg/kg nimodipine (I/R+10 mg/kg NM). The relative expression of LRG1, TGF-β1, p-SMAD2/SMAD, p-SMAD3/SMAD3, ROCK1, p-mTOR/mTOR, occludin, claudin-5, ZO-1, and β-actin was analyzed. Data were averages ± SD, n = 8. $^{\#\#}p < 0.01$, $^{\#}p < 0.05$ *vs.* sham-operated mice, $^{**}p < 0.01$, $^{*}p < 0.05$ *vs.* 1 h of ischemia, 24 h of reperfusion stroke.

Using WGCNA. We constructed the gene co-expression network based on the correlation coefficient. Genes/proteins with close relationships through threshold value were delimited and then divided into a closely related module. Different modules were endowed with characteristic values and different colors. Hub modules related to biological problems were screened through the expression mode and function of modules. WGCNA detected 697 unique differentially expressed genes in tonsil allergen sensitization induction, while interleukin (IL)-17 and its regulatory toll-like receptor signaling pathway are more focused on aeroallergen sensitized patients (Hanif *et al.*, 2023). The receiver operating characteristic curves of the four genes through WGCNA demonstrated that these four genes play a critical role and cytoplasmic FMR1 interacting protein 2 (CYFIP2) is strongly associated with the prognosis of patients with rheumatoid arthritis and tumors (Zhao *et al.*, 2022). Cancer-associated fibroblast hub genes have been filtered via WGCNA to construct a prognostic signature for ovarian cancer (Feng *et al.*, 2022). Thus, WGCNA is an advantageous tool to help identify key genes from the vast network.

WGCNA revealed that 952 differential expression proteins were included in the hub module. Therefore, targeted proteins screened by WGCNA might also play a critical role in cerebral I/R. The enriched signaling pathway should be consistent with GO findings. TGF-β is a member of a superfamily, whose most biological jobs include the regulation of cell growth and differentiation; over a third portion of functions were associated with TGF-β1. Human TGF-β1 is localized on chromosome 19q13 and expressed in endothelial cells and connective tissue cells, which affects the regeneration of vascular endothelial cells, epithelial cells, and the hematopoietic system. Here, from the hub protein network, targets of TGFBI, TGFBR2, TGFB1I1, and TGFBRAP1 exhibited high connectivity in the network. Combining SMAD1, SMAD2, SMAD5, SMAD7, and SMAD9 data revealed a close association between GO and KEGG signaling pathway analyses. BP was related to the TGF-β receptor signaling pathway, positive regulation of transcription, SMAD protein signal transduction, etc., while the predicted KEGG signaling pathway was associated to the TGF-β signaling pathway. The activation of the TGF-β/SMAD2/3 signaling pathway increases the release of vascular endothelial growth factor and thus promoted angiogenesis in ischemic stroke brain (Zhang *et al.*, 2022). TGF-β activity plays a key role in mediating neuroplasticity and recovery of neural function through growth arrest and inducing DNA damage after cerebral I/R injury (Zhang *et al.*, 2019). Macrophage inflammatory cascade caused by

stroke increased swarming of inflammatory cytokine levels of IL-1β, IL-6, monocyte chemoattractant protein-1 (MCP-1), and TGF-β in the heart might contribute to post-stroke cardiac dysfunction (Yan *et al.*, 2020).

TGF-β is connected with variation in the tight junction and offers a new way to induce exosomal lnc-MMP2-2 to increase the barrier-blood brain permeability to promote brain metastasis due to non-small-cell lung cancer (Wu *et al.*, 2021). Up-regulation of the TGF-β mRNA expression demonstrated barrier-blood brain damage and neurobehavioral changes induced by methyl mercury in the rat cerebellum (Abu-Zeid *et al.*, 2021). Platelet-derived growth factor receptor-α effects might be mediated through TGF-β1, which has a protective effect on the barrier-blood brain (Nguyen *et al.*, 2021). It has also been reported that SMAD2 might be involved in the pathological process of ischemic stroke. Stem cell-derived small extracellular vesicles induce a marked increase in regulatory T cells, while the process depends upon activated TGF-β/SMAD through the transmission of TGF-β, SMAD2, and SMAD4 (Xia *et al.*, 2021). In another study, barrier-blood brain integrity suffered and was destroyed at 12 and 24 h after middle cerebral artery occlusion (MCAO), and the levels of TGF-β1, TGF-βR(II), and p-SMAD2/3 were up-regulated (Yang *et al.*, 2021b) In this study, *D. odorifera* leaves could attenuate the blood-brain barrier damage, accompanied by TGF-β1 activation and the phosphorylation of SMAD2. Additionally, through western blot assay, we confirmed some potential upstream and downstream targets.

In addition to the TGF-β signaling pathway, we found that focal adhesion and adherens junction were also the predicted signaling pathway. Focal adhesion and adherens junction are the essential ingredients for the blood-brain barrier integrity. Adhesive junctions form “grid” and “lock” shaped tight junctions that maintain the internal environment of brain tissues by preventing the molecules from invading. Previous studies have reported that focal adhesion (Yang *et al.*, 2022) and adherens junction (Cai *et al.*, 2022) have an important function in the blood-brain barrier. Thus, in this study, we conducted the evaluation of blood-brain barrier permeability to verify the focal adhesion and adherens junction pathway and found that the tight junction proteins, occludin, claudin-5, and ZO-1 were downregulated after cerebral I/R, while DLE could restore the downregulation of tight junctions. Also, the pathological staining, immunofluorescence, and western blotting results were in accordance with the Evans blue staining. The WGCNA prediction results agreed well with the experimental observations.

The top ten scoring signaling pathway included oxidative stress, autophagy and apoptosis-associated pathway, MAPK signaling pathway, mTOR signaling pathway, and apoptosis. The hub proteins MAPK3, mTOR, and ROCK1 play an important role in the regulation of cerebral I/R (Xu *et al.*, 2021). Also, the phosphatidylinositol phosphate 3-kinase-Akt signaling pathway (related hub genes: *AKT1* and *PIK3CA*) tends to be a protective pathway, activated after the stimulation of cerebral I/R (Li *et al.*, 2023). In addition, other signaling pathways tightly associated with stroke were the chemokine signaling pathway (related hub gene: *NOS3*), related to the release of inflammatory factors; the platelet activation signaling pathway (related hub gene: *IGF1R*) is associated with hyperactivation of clotting function, while the VEGF signaling pathway is relevant to abnormal neovascularization. The literature suggests that these pathways and hub targets closely related to stroke. Due to the limited experimental condition, the more specific experiments could not be verified and need to be confirmed in the future.

LRG1 belongs to the leucine-rich repeat family, containing eight leucine-rich repeats. The *LRG1* gene is located on chromosome 19P13.3, with a predicted molecular weight of 38 kD. The vast majority of leucine-rich repeat proteins that have been highly expressed in the nervous system are transmembrane proteins, primarily involved with the formation of the synapse, the growth of neuroprocesses, and the release of neurotransmitters as cell adhesion molecules or interacting proteins (Zhang *et al.*, 2021). There are only a few experimental reports regarding LRG1 and cerebral I/R. LRG1 also exacerbated I/R injury by promoting apoptosis and autophagy via regulating the TGFβ-SMAD1/5 signaling pathway (Jin *et al.*, 2019). Overexpression of LRG1 aggravated cerebral infarction in MCAO rats, enhancing apoptosis and autophagy in the brain tissue (Yamashita *et al.*, 2010). In the MCAO mouse model, LRG1 promoted endothelial cell mitosis and angiogenesis via the activation of the TGF-β pathway (Meng *et al.*, 2016; Cao *et al.*, 2020; Pek *et al.*, 2015). There are only a few reports on the relationship between LRG1 and the tight junction. Studies have shown that LRG1 could regulate the TGF-β signaling pathway (Nakajima *et al.*, 2012); DLE might exert its functions through the LRG1/TGF-β signaling pathway.

This study has certain limitations. Further attempts for experimental verification of the mechanism of other predicted pathways and hub targets might be valuable. Although experiment verification was restricted in the research, we believe the TGF-β signaling pathway is highly correlated with ischemia stroke.

Conclusion

It is evident that an in-depth study of proteins would help to understand the mechanism of the occurrence of I/R and its biological functions. The integrated method used in this study identified the differentially expressed proteins in I/R based on DLE via WGCNA. The exploitation of *D. odorifera* leaves has great potential economic and environmental value because of its role in the attenuation of blood-brain barrier damage induced by I/R; furthermore, the attenuation mechanism is associated with the regulation of the LRG1/TGF-β signaling pathway.

Acknowledgement: We kindly acknowledge Jiangxi University of Traditional Chinese Medicine for providing the *D. odorifera* leaves.

Funding Statement: This work was supported by National Natural Science Foundation of China (Nos. 82100417, 81760094, 81760724); The Foundation of Jiangxi Provincial Department of Science and Technology Project (Nos.

20202ACBL206001, 20212BAB206022, 20181BAB205026); Youth Project of Jiangxi Education Department (No. GJJ200217); Open Project of Key Laboratory of Modern of TCM, Ministry of Education Jiangxi University of Traditional Chinese Medicine (TCM-2019010). The funders had no role in the study design, data collection, analysis, or the decision to publish or prepare the manuscript.

Author Contributions: Jinfang Hu and Jiangen Ao wrote the manuscript. Longsheng Fu, Yaoqi Wu, Feng Shao, Tiantian Xu, Mingjin Jiang, and Shaofeng Xiong conducted the experiment and analyzed the experimental data. Yanni Lv wrote the manuscript and made the final complement.

Availability of Data and Materials: All data generated or analyzed during this study are included in this published article.

Ethics Approval: The experimental protocol was established according to the ethical guidelines and was approved by the Ethics Committee of The First Affiliated Hospital of Nanchang University.

Conflicts of Interest: The authors declare that they have no conflicts of interest to report regarding the present study.

Supplementary Materials: The supplementary material is available online at DOI: 10.32604/biocell.2023.028684.

References

Abu-Zeid EH, Khalifa BA, Elewa YHA, Arisha AH, Ismail TA, Hendam BM, Abdel-Hamid SE (2021). Bee venom *Apis mellifera lamarckii* rescues blood brain barrier damage and neurobehavioral changes induced by methyl mercury via regulating tight junction proteins expression in rat cerebellum. *Food and Chemical Toxicology* **154**: 112309. https://doi.org/10.1016/j.fct.2021.112309

Cai N, Xu B, Li X, Qin Y, Li M, Chen K, Xu J, Wang H (2022). Roflumilast, a cyclic nucleotide phosphodiesterase 4 inhibitor, protects against cerebrovascular endothelial injury following cerebral ischemia/reperfusion by activating the Notch1/Hes1 pathway. *European Journal of Pharmacology* **926**: 175027. https://doi.org/10.1016/j.ejphar.2022.175027

Cao JW, Zhong D, Li GZ (2020). LRG1 and TGF after cerebral ischemia in mice-β1. *Journal of Brain and Neurological Diseases* **28**: 595–600.

Feng S, Xu Y, Dai Z, Yin H, Zhang K, Shen Y (2022). Integrative analysis from multicenter studies identifies a WGCNA-derived cancer-associated fibroblast signature for ovarian cancer. *Frontiers in Immunology* **13**: 951582. https://doi.org/10.3389/fimmu.2022.951582

Hanif T, Ivaska LE, Ahmad F, Tan G, Mikola E, Puhakka T, Palomares O, Akdis CA, Toppila-Salmi S, Jartti T (2023). Tonsillar transcriptional profiles in atopic and non-atopic subjects. *Allergy* **78**: 522–536. https://doi.org/10.1111/all.15458

Jin J, Sun H, Liu D, Wang H, Liu Q, Chen H, Zhong D, Li G (2019). LRG1 promotes apoptosis and autophagy through the TGFβ-smad1/5 signaling pathway to exacerbate ischemia/reperfusion injury. *Neuroscience* **413**: 123–134. https://doi.org/10.1016/j.neuroscience.2019.06.008

Li JY, Chen DL (2013). Antioxidant activity of the extracts from *Dalbergia odorifera* T. Chen leaves in vitro. *Medicinal Plant* **4**: 58–61.

Li F, Duan J, Zhao M, Huang S, Mu F et al. (2019). A network pharmacology approach to reveal the protective mechanism of Salvia miltiorrhiza-*Dalbergia odorifera* coupled-herbs on coronary heart disease. *Scientific Reports* **9**: 19343. https://doi.org/10.1038/s41598-019-56050-5

Li L, Liu JZ, Luo M, Wang W, Huang YY, Efferth T, Wang HM, Fu YJ (2016). Efficient extraction and preparative separation of four main isoflavonoids from *Dalbergia odorifera* T. Chen leaves by deep eutectic solvents-based negative pressure cavitation extraction followed by macroporous resin column chromatography. *Journal of Chromatography B* **1033–1034**: 40–48. https://doi.org/10.1016/j.jchromb.2016.08.005

Li Z, Xiao G, Wang H, He S, Zhu Y (2021). A preparation of *Ginkgo biloba* L. leaves extract inhibits the apoptosis of hippocampal neurons in post-stroke mice via regulating the expression of Bax/Bcl-2 and Caspase-3. *Journal of Ethnopharmacology* **280**: 114481. https://doi.org/10.1016/j.jep.2021.114481

Li R, Zheng Y, Zhang J, Zhou Y, Fan X (2023). Gomisin N attenuated cerebral ischemia-reperfusion injury through inhibition of autophagy by activating the PI3K/AKT/mTOR pathway. *Phytomedicine* **110**: 154644. https://doi.org/10.1016/j.phymed.2023.154644

Lv Y, Fu L (2018). The potential mechanism for Hydroxysafflor yellow A attenuating blood-brain barrier dysfunction via tight junction signaling pathways excavated by an integrated serial affinity chromatography and shotgun proteomics analysis approach. *Neurochemistry International* **112**: 38–48. https://doi.org/10.1016/j.neuint.2017.10.012

Ma RK, Liu H, Shi F, Fu Y, Wei P (2020). The chemical composition and antioxidant activity of essential oils and extracts of *Dalbergia odorifera* leaves. *Holzforschung* **74**: 755–763. https://doi.org/10.1515/hf-2019-0155

Mei H, Hu H, Lv Y, Ma G, Tang F, Hong Z, Shao F (2021). The hypolipidemic effect of *Dalbergia odorifera* T. C. Chen leaf extract on hyperlipidemic rats and its mechanism investigation based on network pharmacology. *Evidence-Based Complementary and Alternative Medicine* **2021**: 3155266.

Meng H, Song Y, Zhu J, Liu Q, Lu P, Ye N, Zhang Z, Pang Y, Qi J, Wu H (2016). LRG1 promotes angiogenesis through upregulating the TGF-β1 pathway in ischemic rat brain. *Molecular Medicine Reports* **14**: 5535–5543. https://doi.org/10.3892/mmr.2016.5925

Nakajima M, Miyajima M, Ogino I, Wada S, Kano T, Kakinuma C, Ogihara T (2012). Brain localization of leucine-rich α2-glycoprotein and its role. *Acta Neurochirurgica Supplementum* **113**: 97–101. https://doi.org/10.1007/978-3-7091-0923-6

Nguyen QL, Okuno N, Hamashima T, Dang ST, Fujikawa M et al. (2021). Vascular PDGFR-alpha protects against BBB dysfunction after stroke in mice. *Angiogenesis* **24**: 35–46. https://doi.org/10.1007/s10456-020-09742-w

Pek SL, Tavintharan S, Wang X, Lim SC, Woon K, Yeoh LY, Ng X, Liu J, Sum CF (2015). Elevation of a novel angiogenic factor, leucine-rich-α2-glycoprotein (LRG1), is associated with arterial stiffness, endothelial dysfunction, and peripheral arterial disease in patients with type 2 diabetes.

The Journal of Clinical Endocrinology and Metabolism **100**: 1586–1593. https://doi.org/10.1210/jc.2014-3855

Sarfraz A, Javeed M, Shah MA, Hussain G, Shafiq N et al. (2020). Biochanin A: A novel bioactive multifunctional compound from nature. *Science of the Total Environment* **722**: 137907. https://doi.org/10.1016/j.scitotenv.2020.137907

Shao F, Gu L, Chen H, Liu R, Huang H, Ren G (2016). Comparation of hypolipidemic and antioxidant effects of aqueous and ethanol extracts of crataegus pinnatifida fruit in high-fat emulsion-induced hyperlipidemia rats. *Pharmacognosy Magazine* **12**: 64–69. https://doi.org/10.4103/0973-1296.176049

Shuai M, He D, Chen X (2021). Optimizing weighted gene co-expression network analysis with a multi-threaded calculation of the topological overlap matrix. *Statistical Applications in Genetics and Molecular Biology* **20**: 145–153. https://doi.org/10.1515/sagmb-2021-0025

Sonoda T, Matsuzaki J, Yamamoto Y, Sakurai T, Aoki Y, Takizawa S, Niida S, Ochiya T (2019). Serum microRNA-based risk prediction for stroke. *Stroke* **50**: 1510–1518. https://doi.org/10.1161/STROKEAHA.118.023648

Wang Y, Liu S, Wang R, Shi L, Liu Z, Liu Z (2020). Study on the therapeutic material basis and effect of Acanthopanax senticosus (Rupr. et Maxim.) Harms leaves in the treatment of ischemic stroke by PK-PD analysis based on online microdialysis-LC-MS/MS method. *Food & Function* **11**: 2005–2016. https://doi.org/10.1039/C9FO02475A

Wu D, Deng S, Li L, Liu T, Zhang T, Li J, Yu Y, Xu Y (2021). TGF-β1-mediated exosomal lnc-MMP2-2 increases blood-brain barrier permeability via the miRNA-1207-5p/EPB41L5 axis to promote non-small cell lung cancer brain metastasis. *Cell Death & Disease* **12**: 721. https://doi.org/10.1038/s41419-021-04004-z

Xia Y, Hu G, Chen Y, Yuan J, Zhang J, Wang S, Li Q, Wang Y, Deng Z (2021). Embryonic stem cell derived small extracellular vesicles modulate regulatory T cells to protect against ischemic stroke. *ACS Nano* **15**: 7370–7385. https://doi.org/10.1021/acsnano.1c00672

Xu D, Kong T, Zhang S, Cheng B, Chen J, Wang C (2021). Orexin-A protects against cerebral ischemia-reperfusion injury by inhibiting excessive autophagy through OX1R-mediated MAPK/ERK/mTOR pathway. *Cellular Signalling* **79**: 109839. https://doi.org/10.1016/j.cellsig.2020.109839

Yamashita F, Sasaki M, Takahashi S, Matsuda H, Kudo K, Narumi S, Terayama Y, Asada T (2010). Detection of changes in cerebrospinal fluid space in idiopathic normal pressure hydrocephalus using voxel-based morphometry. *Neuroradiology* **52**: 381–386. https://doi.org/10.1007/s00234-009-0610-z

Yan T, Chen Z, Chopp M, Venkat P, Zacharek A et al. (2020). Inflammatory responses mediate brain-heart interaction after ischemic stroke in adult mice. *Journal of Cerebral Blood Flow and Metabolism* **40**: 1213–1229. https://doi.org/10.1177/0271678X18813317

Yang J, Hao J, Lin Y, Guo Y, Liao K, Yang M, Cheng H, Yang M, Chen K (2022). Profile and functional prediction of plasma exosome-derived circRNAs from acute ischemic stroke patients. *Frontiers in Genetics* **13**: 810974. https://doi.org/10.3389/fgene.2022.810974

Yang R, Jia Q, Mehmood S, Ma S, Liu X (2021a). Genistein ameliorates inflammation and insulin resistance through mediation of gut microbiota composition in type 2 diabetic mice. *European Journal of Nutrition* **60**: 2155–2168. https://doi.org/10.1007/s00394-020-02403-0

Yang X, Liang J, Jia M, Yang T, Deng X et al. (2021b). β-1, 3-galactosyltransferase 2 ameliorates focal ischemic cerebral injury by maintaining blood-brain barrier integrity. *Neurochemistry International* **144**: 104976. https://doi.org/10.1016/j.neuint.2021.104976

Zhang Y, Mu Y, Ding H, Du B, Zhou M, Li Q, Gong S, Zhang F, Geng D, Wang Y (2022). 1α,25-dihydroxyvitamin D3 promotes angiogenesis after cerebral ischemia injury in rats by upregulating the TGF-β/Smad2/3 signaling pathway. *Frontiers in Cardiovascular Medicine* **9**: 769717. https://doi.org/10.3389/fcvm.2022.769717

Zhang M, Wang Y, Wang J, Li X, Ma A, Pan X (2021). Serum LRG1 as a novel biomarker for cardioembolic stroke. *Clinica Chimica Acta; International Journal of Clinical Chemistry* **519**: 83–91. https://doi.org/10.1016/j.cca.2021.04.002

Zhang K, Zhang Q, Deng J, Li J, Li J, Wen L, Ma J, Li C (2019). ALK5 signaling pathway mediates neurogenesis and functional recovery after cerebral ischemia/reperfusion in rats via Gadd45b. *Cell Death & Disease* **10**: 360. https://doi.org/10.1038/s41419-019-1596-z

Zhao Z, He S, Yu X, Lai X, Tang S et al. (2022). Analysis and experimental validation of rheumatoid arthritis innate immunity gene CYFIP2 and pan-cancer. *Frontiers in Immunology* **13**: 954848. https://doi.org/10.3389/fimmu.2022.954848

Supplementary Materials

Table S1. Identified proteins from cerebral I/R mice treated with control-affinity resin via series affinity chromatography

Table S2. Identified proteins from cerebral I/R mice treated with DLE (70% ethanol extract of *D. odorifera* leaves)-affinity resin via series affinity chromatography

Table S3. Differential expression proteins for each band screened with the criteria of $\log_2$Fold Change > 0.5, adj.*p*.Val < 0.05 based on the comparison between identified proteins from cerebral I/R mice treated with control-affinity resin and DLE-affinity resin via series affinity chromatography

Figure S1. Volcano map of differential expression proteins based on the comparison between identified proteins from cerebral I/R mice treated with control-affinity resin and DLE-affinity resin via series affinity chromatography.